ISSN 1063-7788, Physics of Atomic Nuclei, 2017, Vol. 80, No. 6, pp. 1106–1118. © Pleiades Publishing, Ltd., 2017.
Original Russian Text © V.V. Varlamov, B.S. Ishkhanov, V.N. Orlin, 2017, published in Yadernaya Fizika, 2017, Vol. 80, No. 6, pp. 632–644.

NUCLEI
Theory

Evaluated Cross Sections of Photoneutron Reactions on the Isotope ^{116}Sn and Spectra of Neutrons Originating from These Reactions

V. V. Varlamov[1)*], B. S. Ishkhanov[1),2)], and V. N. Orlin[1)]

Received May 24, 2017

Abstract—With the aid of the results obtained by evaluating cross sections of partial photoneutron reactions on the isotope ^{116}Sn and the energy spectra of neutrons originating from these reactions, the possible reasons for the well-known discrepancies between the results of different photonuclear experiments were studied on the basis of a combined model of photonuclear reactions. On the basis of physical criteria of data reliability and an experimental–theoretical method for evaluating cross sections of partial reactions, it was found that these discrepancies were due to unreliably redistributing neutrons between $(\gamma, 1n)$, $(\gamma, 2n)$, and $(\gamma, 3n)$ reactions because of nontrivial correlations between the experimentally measured energy of neutrons and their multiplicity.

DOI: 10.1134/S1063778817060230

1. INTRODUCTION

Investigation of the mechanism of photon interaction with nuclei is one of the priority lines of research in nuclear physics. A feature peculiar to photon interaction with nuclei is their intense absorption in the energy range between 8 and 20 MeV—a giant dipole resonance (GDR). The GDR phenomenon is observed in all nuclei, without exception. For the first time, it was predicted by A.B. Migdal [1] and was experimentally observed by Baldwin and Klaiber in ^{238}U photofission [2] and in photoneutron reactions on the isotopes ^{12}C and ^{63}Cu [3]. In collective models of the nucleus, the giant dipole resonance is interpreted as the vibration of all intranuclear protons with respect to all intranuclear neutrons in photon absorption by the nucleus being considered [4]. Within the collective models, it turned out to be possible to relate GDR properties to fundamental properties of the nucleus such as its radius and mass and the numbers of neutrons, N, and protons, Z, in it. In particular, the resonance-maximum position E_m and the total cross section of photon interaction with the nucleus depend on the number of nucleons, A, in the nucleus, $A = N + Z$; that is,

$$E_m = h\omega \approx 78A^{-1/3}\ [\text{MeV}], \qquad (1)$$

$$\int\limits_{\text{GDR}} \sigma d\omega \approx 60\frac{NZ}{A}\ [\text{MeV mb}]. \qquad (2)$$

The prediction and subsequent discovery of splitting of the maximum of the giant resonance in deformed nuclei that corresponds to nuclear-matter vibrations along the axes of the nuclear ellipsoid [5, 6] were undoubtedly a success of collective models.

The advent of the shell model made it possible to interpret GDR states as photon-induced nucleon transitions from occupied to unoccupied nuclear shells. For the first time, such an interpretation was proposed by Wilkinson [7]. However, the resonance-maximum position determined theoretically in his study proved to be lower on the energy scale by a factor of about two than its experimental counterpart. The next important step in developing the shell model of giant dipole resonances involved taking into account the residual particle–hole interaction of intranuclear nucleons [8–10]. Not only did the position of the GDR maximum prove to be fully in agreement with experimental data, but it also explained the nature of collective nucleon vibrations in nuclei [9]. The residual nucleon–nucleon interaction led to the formation of a dipole state that stood out as a coherent superposition of single-particle transitions.

Experimental methods for studying giant dipole resonances have also underwent substantial changes. In nature, there are no monoenergetic sources of 10- to 30-MeV photons. Therefore, the first experiments devoted to studying giant dipole resonances were performed in bremsstrahlung beams. A beam of accelerated electrons was incident to a target from

[1)]Skobeltsyn Institute of Nuclear Physics, Moscow State University, Moscow, 119991 Russia.
[2)]Faculty of Physics, Moscow State University, Moscow, 119991 Russia.
[*]E-mail: Varlamov@depni.sinp.msu.ru

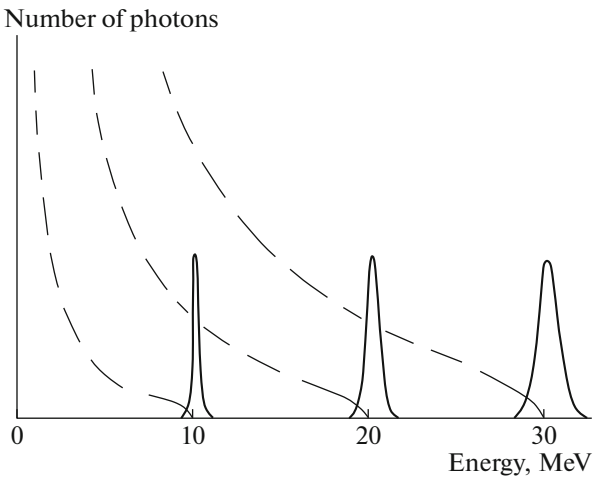

Fig. 1. Spectra of photons (in relative units number) produced upon the exposure of a beryllium target to 10-, 20-, and 30 MeV electrons and positrons. The dashed and solid curves represent, respectively, bremsstrahlung spectra and spectra of quasimonoenergetic photons originating from positron annihilation.

a large-Z material, and this led to the production of photons whose spectrum was continuous, extending to the endpoint energy $E^{\max}$ equal to the kinetic energy of accelerated electrons (see Fig. 1). Measuring the photonuclear-reaction yield $Y(E^{\max})$ at various values of the endpoint energy $E^{\max}$ and knowing the function describing the bremsstrahlung-spectrum shape, $W(E^{\max}, E_\gamma)$, one can unfold the reaction cross section $\sigma(E_\gamma)$ by means of the relation

$$Y(E^{\max}) = \alpha \int\limits_{E_{\rm thr}}^{E^{\max}} W(E^{\max}, E_\gamma)\sigma(E_\gamma)dE_\gamma, \quad (3)$$

where α is a normalization constant.

Despite the development of various methods for unfolding the reaction cross section from the reaction yield, there remained many problems as to whether the respective solutions of the integral equation (3) are quite reliable.

The next important step in photonuclear studies was due to the creation of beams of quasimonoenergetic photons produced by the annihilation of accelerated positrons on a target from a small-Z material [11, 12]. Facilities of this type were constructed at several laboratories worldwide. The largest amounts of data were obtained in Saclay (France) and in Livermore (USA). The spectra of quasimonoenergetic annihilation photons are shown in Fig. 1. For a more detailed description of the procedure for obtaining quasimonoenergetic photons, the interested reader is referred to [13, 14].

Concurrently, methods for detecting photonuclear-reaction products were improved. In medium-heavy and heavy nuclei, the giant dipole resonance decays predominantly via neutron emission. A large-volume scintillation detector viewed by many photomultiplier tubes was used in Saclay as a detector of photoneutrons originating from photonuclear reactions. In Livermore, neutrons were first moderated and then detected by 48 BF_3 counters arranged as concentric rings around a target within a large paraffin cube.

The creation of beams of quasimonoenergetic photons and highly efficient neutron detectors changed qualitatively the situation in studies of photonuclear reactions and made it possible to obtain new information about the decay features of giant dipole resonances—that is, cross sections of partial reactions involving the emission of various numbers of nucleons. In medium-heavy and heavy nuclei, the total photon-absorption cross section $\sigma(\gamma, abs)$ is in fact determined by the neutron-emission decay channels; that is,

$$\sigma(\gamma, abs) \approx \sigma(\gamma, Sn) = \sigma(\gamma, 1n) \quad (4)$$
$$+ \sigma(\gamma, 1n1p) + \sigma(\gamma, 2n) + \sigma(\gamma, 2n1p)$$
$$+ \sigma(\gamma, 3n) + ...$$

In experiments that employ a beam of bremsstrahlung photons, one determines directly the cross section of the neutron-yield reaction; that is,

$$\sigma(\gamma, Xn) = \sigma(\gamma, 1n) + \sigma(\gamma, 1n1p) \quad (5)$$
$$+ 2\sigma(\gamma, 2n) + 2\sigma(\gamma, 2n1p) + 3\sigma(\gamma, 3n) + ...$$

The majority of experiments aimed at determining cross sections of partial photoneutron reactions were performed by employing quasimonoenergetic annihilation photons at the Lawrence Livermore National Laboratory (USA) and at the Nuclear Research Centre in Saclay (France). In both laboratories, use was made of methods for photoneutron multiplicity sorting that are based on the assumption that the multiplicity of neutrons is directly related to their mean kinetic energy. A large number of cross sections of photoneutron reactions on several tens of various isotopes were measured [15]. These data were included in various reference books and compilations and are extensively used both in fundamental and in applied investigations. However, discrepancies between cross sections obtained for $(\gamma, 1n)$, $(\gamma, 2n)$, and $(\gamma, 3n)$ reactions in beams of quasimonoenergetic photons at different laboratories were noticed before long [16-20].

An analysis of the cross sections of partial photoneutron reactions on 19 nuclei studied at the above two laboratories revealed [18–20] that there are systematic discrepancies between the results of the different experiments.

Although the neutron-yield cross sections in (5), which are unaffected by problems associated with

Table 1. Thresholds for photonuclear reactions on the isotope ^{116}Sn

Reaction	$(\gamma, 1n)$	$(\gamma, 2n)$	$(\gamma, 1p)$	$(\gamma, 1p1n)$	$(\gamma, 3n)$
$E_{\rm thr}$ [MeV]	9.56	17.10	9.27	18.30	27.42

neutron multiplicity sorting, show rather good agreement, the Livermore and Saclay data on the cross sections of $(\gamma, 1n)$ and $(\gamma, 2n)$ partial reactions are different. Moreover, the $(\gamma, 2n)$ cross sections are larger in Livermore than in Saclay, while the $(\gamma, 1n)$ cross sections are smaller in Livermore than in Saclay. As a result, the Livermore/Saclay cross-section ratios are greater than unity (about 1.1) for the $(\gamma, 2n)$ reactions and are substantially less than unity (about 0.8) for the $(\gamma, 1n)$ reactions. This means that the distinctions under discussion between the cross sections of photoneutron reactions have a systematic character. These discrepancies may be as large as about 60 to 100%.

It was shown that the observed discrepancies are due primarily to the systematic errors of the method for determining the multiplicity of neutrons emitted in various reactions on the basis of their measured kinetic energy. These errors lead to the redistribution of some neutrons among channels that have different multiplicities. As a result, part of the $(\gamma, 1n)$ cross section is misidentified as the $(\gamma, 2n)$ cross section, or vice versa. According to our estimates, the misidentified part of the $(\gamma, 2n)$ cross section is about 20%. As a result, the $(\gamma, 1n)$ cross sections decrease, developing physically forbidden negative values, while the $(\gamma, 2n)$ cross sections increase.

Experimental information about GDR decay channels gave impetus to developing new theoretical models that described in more detail manifestations of various properties of the giant dipole resonance [21–27], and this required a more accurate reanalysis of experimental data.

In the present study, the possible reasons for the aforementioned discrepancies are discussed on the basis of an analysis of cross sections of photoneutron reactions on the isotope ^{116}Sn.

2. EXPERIMENTAL METHOD

Table 1 lists the thresholds for basic photonuclear reactions on the isotope ^{116}Sn.

The cross sections of photoneutron reactions on the isotope ^{116}Sn were measured both in beams of bremsstrahlung photons [28] and in beams of quasimonoenergetic photons [29, 30]. The most important features of these cross sections from the compilation in [31] are given in Table 2.

A comparison of the features of the measured cross sections shows that there is good agreement for the position of the GDR maximum, E^m, and for the cross section at the resonance maximum, σ^m, but that the measured resonance widths are strongly different. For example, the difference in the width of the cross sections of the (γ, Xn) and (γ, Sn) reactions according to the Saclay and Livermore data is about 1.5 MeV. The splitting of the resonance maximum and additional maxima at the energies of 18.769 and 27.131 MeV were discovered in the Livermore experiments [29]. Similar features were also found in the cross sections of the $(\gamma, 1n)$ and $(\gamma, 2n)$ partial channels.

Below, we will discuss in more detail the results obtained the Livermore experiments [29].

The cross sections of photoneutron reactions were measured in a beam of quasimonoenergetic photons in the energy range from the threshold for the $(\gamma, 1n)$ photoneutron reaction to about 30 MeV.

The quasimonoenergetic photons originated from the process of positron annihilation on a beryllium target. In this process, the emission of two photons at angles of 0° and 180° with respect to the positron momentum is the most probable. The photon flying at an angle of 0° carries away almost the whole amount of the positron energy E^+; that is,

$$E_\gamma = E^+ + mc^2/2. \qquad (6)$$

The spectrum of photons produced upon the exposure of a beryllium target to positrons of energy $E^+ = 10$, 20, and 30 MeV is shown in Fig. 1.

The spectrum of annihilation photons is accompanied by the spectrum of bremsstrahlung from positrons in the beryllium target; therefore, measurements of the photoneutron-reaction cross sections $\sigma(E_\gamma)$ were performed in three steps. First, the yield $Y^+(E^+)$ of the reaction induced by a beam of photons produced upon the exposure of the beryllium target to positrons of energy E^+ was measured. The spectrum contains both annihilation and bremsstrahlung photons. After that, the yield $Y^-(E^-)$ was measured for the analogous reaction induced in the case where the same number of electrons with the same energy hit the beryllium target. It was assumed that the properties of bremsstrahlung from positrons and electrons are identical.

For the measured cross sections, one takes the difference

$$\sigma(E_\gamma) = Y^+(E^+) - Y^-(E^-). \qquad (7)$$

In Fig. 2, examples of neutron yields from a target irradiated with a beam of photons produced on a beryllium target exposed to (Fig. 2*a*) positrons and

Table 2. Cross sections of photoneutron reactions on the isotope ^{116}Sn

Reaction	Position of the cross-section maximum, E^m, MeV	Cross section at the maximum, σ^m, mb	Resonance width Γ, MeV	Upper boundary for the integrated cross section, MeV	Integrated cross sections, MeV mb	References
(γ, Xn)	15.6	260.0	9.0	27.00	2400	[28]
	15.44	277.3	7.5	22.10	1823	[30]
	15.362	272.0	6.0	29.60	2083	[29]
	18.769	168.9				
	27.131	76.0				
(γ, Sn)	15.6	260.0	6.0	27.00	2850	[28]
	15.44	277.3	7.5	29.50	1630	[30]
	15.982	262.0	4.0	29.60	1669	[29]
	27.131	55.0				
$(\gamma, 1n)$	15.44	277.3	7.5	22.10	1437	[30]
	15.362	272.0	3.5	29.60	1255	[29]
	28.37	36.0				
$(\gamma, 2n)$	20.07	51.4	>7.0	22.10	193	[30]
	20.008	60.0	7.5	29.60	414	[29]

(Fig. 2*b*) electrons are given along with (Fig. 2*c*) the cross sections of the neutron-yield reaction.

The energy resolution of the method that employs quasimonoenergetic photons depends on the energy resolution of the positron beam; multiple positron scattering in the beryllium target; and the accuracy of the absolute normalization of the spectra of bremsstrahlung from positrons and electrons, since the errors in the absolute normalization lead to the formation of the low-energy section of the photon spectrum (dashed line in Fig. 2*c*), the role of these photons is especially important in measuring cross sections at energies in excess of the energy corresponding to the giant-resonance maximum.

The energy resolution of the experiments in question depended on E^+, amounting to 300 keV at $E^+ =$ 10 MeV and increasing to 400 keV at $E^+ = 30$ MeV.

After moderation in paraffin, the product neutrons were detected by discharge counters. On the axis of the detector, which was a paraffin cube of size length 61 cm, there was a channel housing a target from the material under study. Forty-eight boron counters containing enriched boron fluoride ($^{10}BF_3$) were arranged on four concentric circles of radius $R = 6.35$, 10.80, 14.61, and 17.78 cm, 12 counters being on each circle.

Signals from each ring of counters were detected independently. The neutrons were detected between gamma-ray pulses within 300 μs. Since the number of the neutrons detected in each ring depended on the distances traveled by each of them in the paraffin moderator and, hence, on their energies, information about neutron energies could be obtained by measuring the number of neutrons detected in each ring. As the photon energy increased from 10 to 24 MeV, the total efficiency of neutron detection by the detector decreased from 43% to 38% (see Fig. 3).

The multiplicity sorting of the reaction yields $Y_i(\gamma, in)$ was based on the results of counting the number of neutrons, N_i, after each pulse of gamma radiation from the accelerator. We restrict our consideration to the case of the $(\gamma, 1n)$ and $(\gamma, 2n)$ reactions. If the mean number of detected neutrons, $\bar{N}$, per accelerator cycle is much less than unity and if the efficiency of neutron detection by the detector is less than unity ($\varepsilon < 1$), then the number of detected neutrons, N_i, and the reaction yield Y_i in the region of energies below the threshold for the $(\gamma, 3n)$ reaction are related by the equations

$$N_1 = \varepsilon Y_1 + 2\varepsilon(\varepsilon - 1)Y_2, \tag{8}$$

$$N_2 = Y_2 \cdot \varepsilon^2. \tag{9}$$

The reaction cross sections $\sigma(\gamma, in)$ were calculated on the basis of the relation

$$\sigma(\gamma, in) = \frac{Y_i}{I}\frac{\mu}{1 - e^{-\mu t}}\frac{1}{\varepsilon^i N_a}, \tag{10}$$

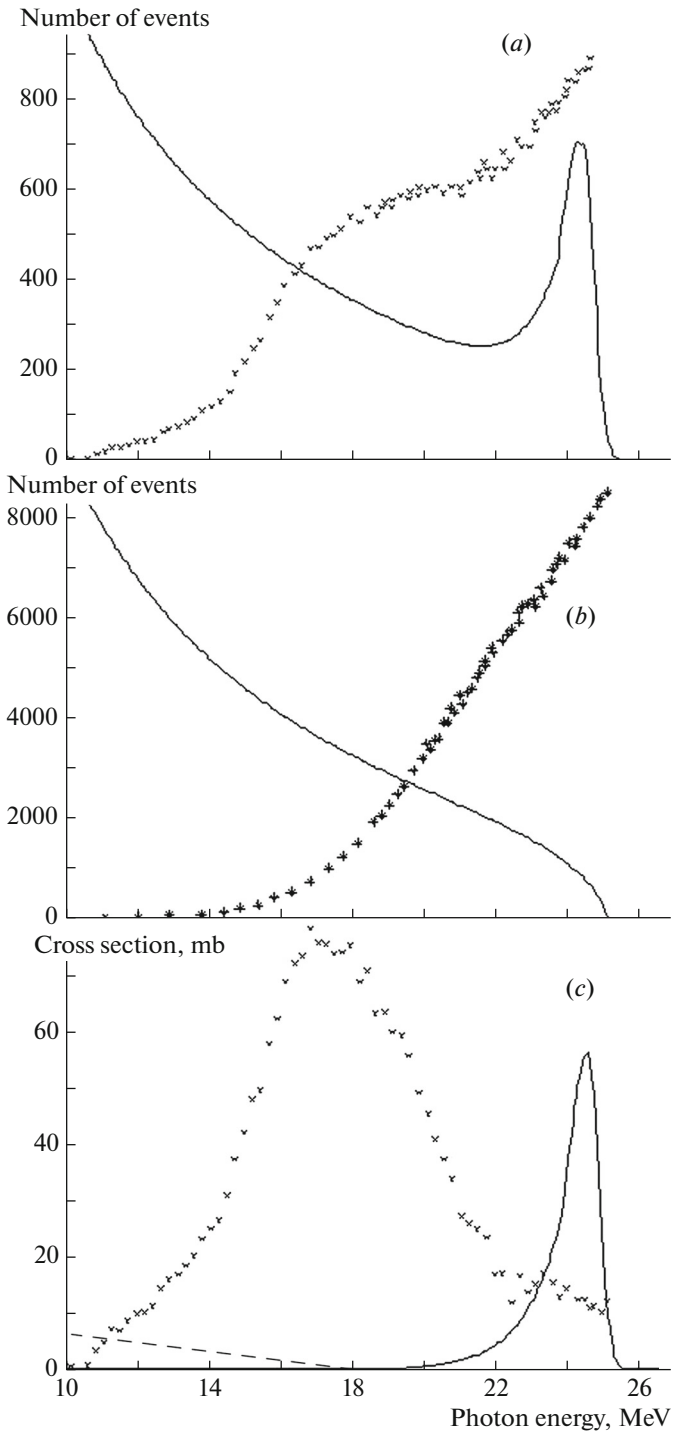

Fig. 2. Three steps of the derivation of information about the photonuclear-reaction cross section in experiments with a beam of quasimonoenergetic annihilation photons: (*a*) measurement of the yield $Y^+(E^+)$ of the reaction induced by annihilation photons and photons of bremsstrahlung generated by positrons, (*b*) measurement of the yield $Y^-(E^-)$ of the respective reaction induced by photons of bremsstrahlung from electrons, and (*c*) determination of the reaction cross section as the difference $Y^+(E^+) - Y^-(E^-)$. The symbols stand for the respective yields and cross section. The curves represent the photon spectra.

where I is the number of quasimonoenergetic photons, N_a is the number of atoms per 1 cm^3 in the target being studied, and $\mu(E_\gamma)$ is the coefficient of absorption of quasimonoenergetic photons in the target.

The dependence of the ratio N_1/N_2 on the energy of photons incident to the target was determined ex-

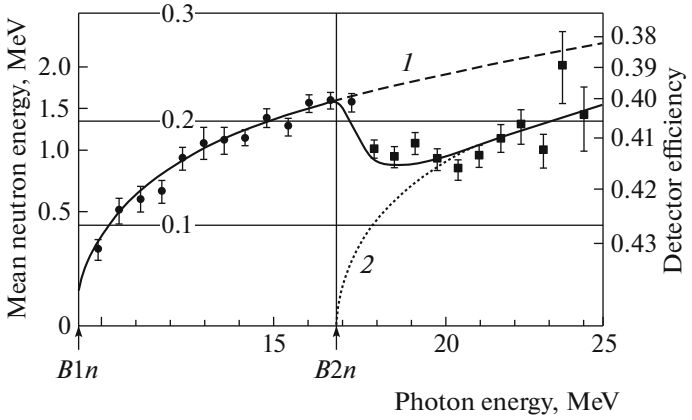

Fig. 3. Dependence of the ring ratios of the neutron-detector efficiencies on the photon energy in experiments with ^{116}Sn nuclei [29] in the (closed circles) energy region extending up to about B2n (the dashed curve corresponds to an interpolation) and (closed boxes) high-energy region (the dotted curve corresponds to an interpolation).

perimentally. On the basis of the known "ring-ratio" calibration curve, this dependence is transformed into the dependence of the mean energy of emitted neutrons on the energy of absorbed photons. After that, the quantity ε appearing in Eqs. (8)–(10) can be determined by using the calibration detector-efficiency curve.

Figures 3 shows the "ring ratios" and the calculated mean neutron energies corresponding to various excitation energies of the isotope ^{116}Sn [29]. One can see a monotonic increase in the mean neutron energy up to 1.5 MeV from the threshold of the $(\gamma, 1n)$ reaction to 17 MeV, which corresponds to the threshold of the $(\gamma, 2n)$ reaction. In the region around 17 MeV, the mean energy of neutrons decreases sharply to 0.8 MeV. The decrease in the mean energy of neutrons at $E_\gamma \approx 17$ MeV is due to the opening of the $(\gamma, 2n)$ reaction channel and, accordingly, to a decrease in the mean energy of neutrons produced in the $(\gamma, 2n)$ reaction. The solid curve ("ring ratio," which reflects the spectrum of neutrons) was plotted on the basis of experimental data; that is,

$$N(E_m) = \text{const} \cdot \left(\frac{E_m}{U^2}\right) \exp(2\alpha U)^{1/2}, \qquad (11)$$

where U is the excitation energy of the final nucleus, E_m is the neutron energy, and $\alpha = 10 \pm 2$ MeV^{-1} is the level-density parameter [which is identical for the $(\gamma, 1n)$ and $(\gamma, 2n)$ reactions].

The dashed and dotted curves represent the ring ratios determined individually for the $(\gamma, 1n)$ and $(\gamma, 2n)$ reactions.

Figure 4 gives the cross sections obtained for various photoneutron reactions in the Livermore and Saclay experiments. We will now compare experimental data obtained in [29–31] with the results of calculations based on the combined photonuclear-reaction model developed in [32, 33].

3. COMBINED MODEL OF PHOTONUCLEAR REACTIONS

In accordance with Bohr's postulate, it is assumed within the combined photonuclear-reaction model [32, 33] that a nuclear reaction has approximately two independent stages: the formation of a compound system and the decay of this system to reaction products. In addition, it is assumed within this model that, for mass numbers ranging from $A \sim 40$ to A values corresponding to transuranium elements, the inclusion of only three competing channels of decay of the compound system in the analysis is quite sufficient. These are decay channels involving neutron, proton, and photon emission.

Up to the pion-production threshold, photoabsorption on a nucleus is determined exclusively by photon interaction with one- and two-nucleon nuclear currents. In the first process, it is assumed that only one nucleon is excited upon the absorption of a photon. This process is dominant in the low-energy region ($E_\gamma < 40$ MeV), where a giant dipole resonance, which is a coherent mixture of single-particle–single-hole $(1p1h)$ excitations, is formed owing to the interaction of electromagnetic interaction with the nucleus being considered. Above this region, the quasideuteron mechanism of photoabsorption comes to be dominant. In this case, the excited nucleon exchanges a virtual pion with a neighboring nucleon, with the result that the energy and momentum of the absorbed photon are transferred to a correlated proton–neutron pair rather than to a single nucleon.

From the experimental data, it follows that, in medium-heavy and heavy nuclei, the giant dipole resonance features one maximum (in spherical nuclei) or two maxima (in deformed nuclei). This means that the energy spread of single-particle dipole transitions

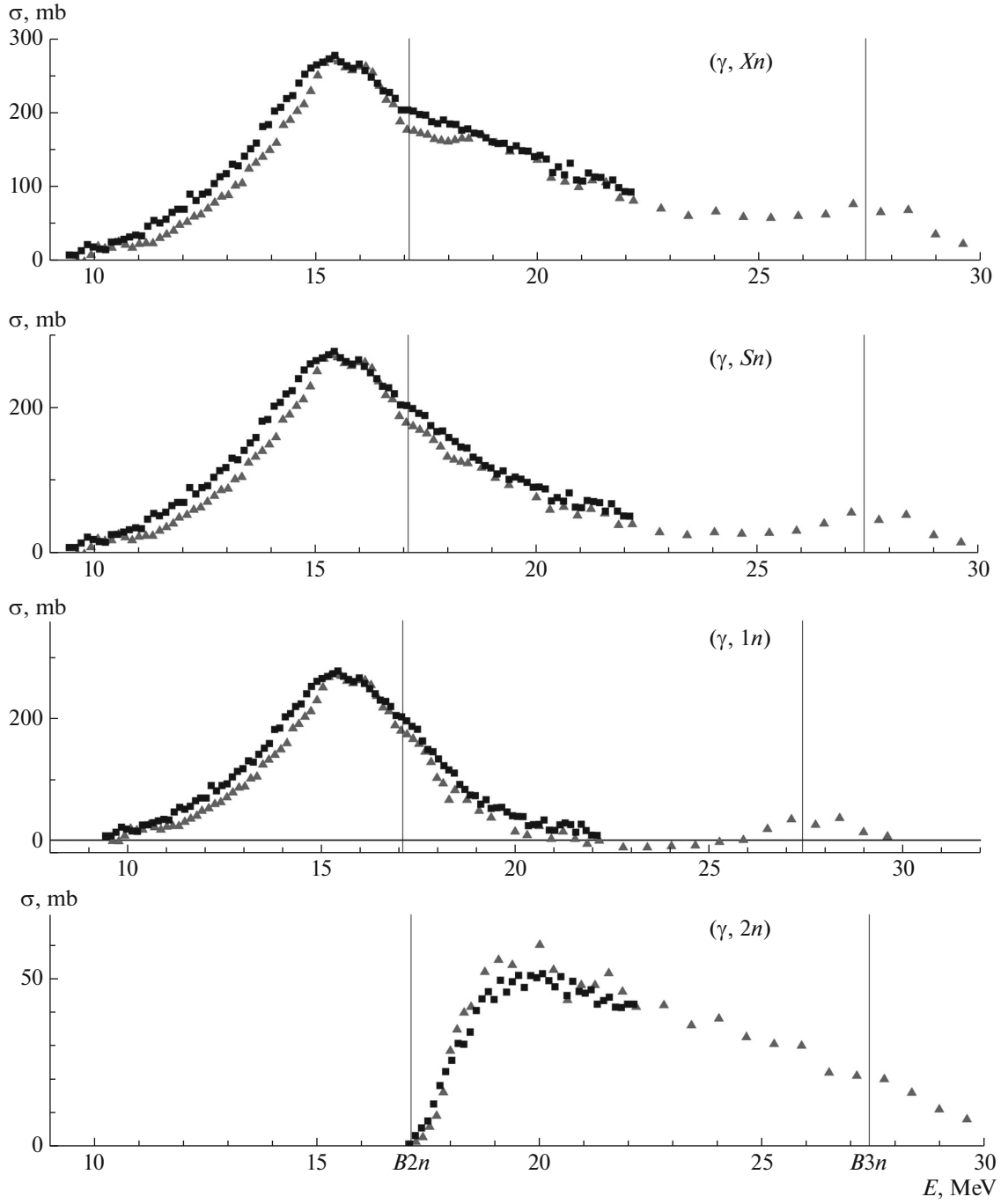

Fig. 4. Cross sections obtained for photoneutron reactions on the ^{116}Sn nucleus in (closed triangles) Livermore [29] and (closed boxes) Saclay [30] experiments.

is small in relation to the residual interaction mixing them. Therefore, a semimicroscopic model of vibrations where basic groups of single-particle transitions are assumed to be degenerate and where the residual interaction is approximated by multipole–multipole forces is used to describe giant resonances within the combined photonuclear-reaction model. The energies and integrated cross sections were calculated within this approach for the giant dipole and isovector giant quadrupole resonances and for the GDR overtone, along with the isospin splitting of the giant dipole resonance. The giant-resonance widths were estimated on the basis of semiempirical expressions.

As was indicated above, the quasideuteron mechanism of photoabsorption is dominant in the energy region of $E > 40$ MeV. The quasideuteron-

mechanism version developed by Chadwick in [34] with allowance for the effect of Pauli blocking on the cross sections of absorption via the quasideuteron mechanism is used within the combined model to describe this process.

As a rule, a combination of the evaporation and preequilibrium (specifically, exciton [35–38]) models of photonucleon reactions is used within the combined photonuclear-reaction model to describe nucleon emission following photon absorption. These models are modified in such a way as to take into account isospin effects. Without this, it is impossible to take correctly into account the competition between the neutron and proton reaction channels, since the $T_>$ component of the giant dipole resonance decays predominantly via proton emission. For medium-heavy and heavy nuclei, this does in fact reduce to replacing, in the exciton and equilibrium densities of the final nucleus, their excitation energy U by $U - \Delta E_T$, where ΔE_T is the excitation energy for the first level of the final nucleus whose isospin is higher by unity than the ground-state isospin of this nucleus.

In preequilibrium models, semidirect photonucleon reactions are usually treated as nucleon emission from a $1p1h$ doorway state. Concurrently, it is assumed that, at a given excitation energy, all $1p1h$ configurations are populated equiprobably, and the effect of the orbital angular, l, and total angular, j, momenta of the excited nucleon on the probability for its emission from the target nucleus is disregarded. This disregard of the shell structure of doorway states leads to an incorrect treatment of the semidirect photoeffect (emission of an excited nucleon directly from a doorway state), and this is especially important in describing the photodisintegration of light and medium-heavy nuclei, where a significant part of photonucleons are emitted in semidirect reactions. In the combined photonuclear-reaction model, the effect exerted by the structure of a doorway state on its decay features is taken into account within the quasideuteron mechanism of absorption, whereby the description of the semidirect photoeffect can be substantially improved. Calculations reveal that this is especially important for nuclei lying far from the beta-stability band on the nuclear map.

In practice, the TALYS multipurpose code is widely used to calculate nuclear reactions. The possibility of including in it a large number of reactions is the main advantage of this code. However, it does not always yield correct results in describing photonucleon reactions because of the disregard of the following three factors: (i) the contribution of the isovector giant quadrupole resonance and the GDR overtone to the photoabsorption cross section, (ii) isospin effects, and (iii) the shell structure of the doorway dipole state.

Figure 5 shows the cross sections calculated on the basis of the combined photonuclear-reaction model for photonucleon reactions on ^{116}Sn nuclei.

4. EVALUATING CROSS SECTIONS OF PHOTONEUTRON REACTIONS ON THE BASIS OF AN EXPERIMENTAL–THEORETICAL METHOD

In accordance with problems arising in experimentally sorting reaction cross sections in multiplicity, it is highly desirable to have an approach to evaluating cross sections of partial photoneutron reactions that is maximally free from these problems. This experimental–theoretical method for evaluating partial-reaction cross sections was proposed in [39, 40]. Within this method, the contribution of partial reactions to the experimental cross section of the neutron-yield reaction is determined with the aid of the transition multiplicity functions

$$F_i^{\text{theor}} = \sigma^{\text{theor}}(\gamma, in)/\sigma^{\text{theor}}(\gamma, Xn) \qquad (12)$$

calculated on the basis of the combined photonuclear-reaction model [32, 33].

The transition functions calculated on the basis of experimental data,

$$F_1^{\text{exp}}(E_\gamma) = \sigma^{\text{exp}}(\gamma, 1n)/\sigma^{\text{exp}}(\gamma, Xn), \qquad (13)$$

$$F_2^{\text{exp}}(E_\gamma) = \sigma^{\text{exp}}(\gamma, 2n)/\sigma^{\text{exp}}(\gamma, Xn), \qquad (14)$$

$$F_3^{\text{exp}}(E_\gamma) = \sigma^{\text{exp}}(\gamma, 3n)/\sigma^{\text{exp}}(\gamma, Xn)\ldots \qquad (15)$$

were first introduced as objective physical criteria of reliability of neutron multiplicity sorting in experiments. By definition, the functions F_1, F_2, F_3, ... cannot take values greater than, respectively, 1.00, 0.50, 0.33, ... The appearance of values of the functions F_1, F_2, F_3, ... in excess of the above absolute limits would mean that the neutron multiplicity sorting was erroneous.

It was shown in [39–41] that the transition multiplicity functions $F_i^{\text{exp}}(E_\gamma)$, obtained on the basis of experimental data provide criteria for a simple, clear-cut, and efficient analysis of the reliability of experimental data on cross sections of partial reactions. It was also shown that, for a large number of nuclei (^{90}Zr, $^{112,114,116-120,122,124}$Sn, ^{159}Tb, and ^{197}Au), experimental data obtained for the $(\gamma, 1n)$, $(\gamma, 2n)$, and $(\gamma, 3n)$ cross sections by means of photoneutron multiplicity sorting do not meet these criteria.

For the aforementioned nuclei, the cross sections of partial photoneutron reactions were evaluated within the experimental–theoretical approach, and the ratios of these cross sections fit in the description on the basis of the combined photonuclear-reaction

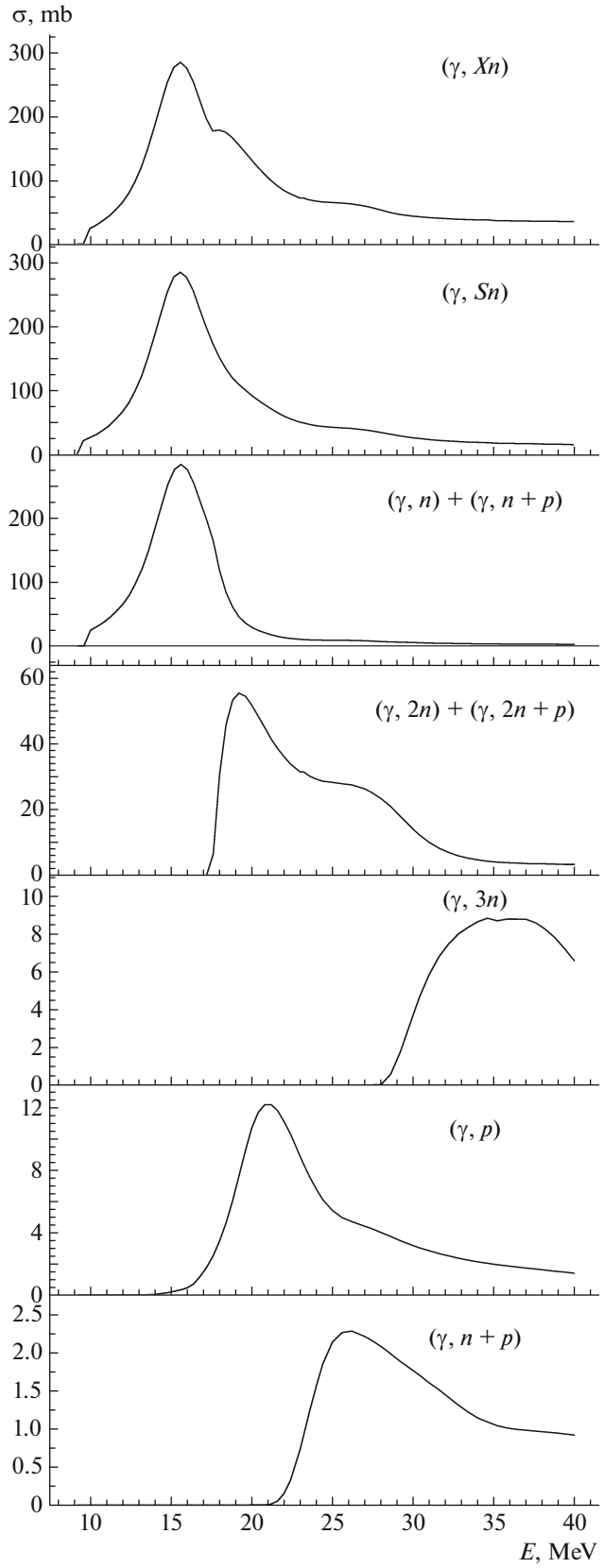

Fig. 5. Cross sections of various photonuclear reactions on ^{116}Sn nuclei according to calculations based on the combined photonuclear-reaction model.

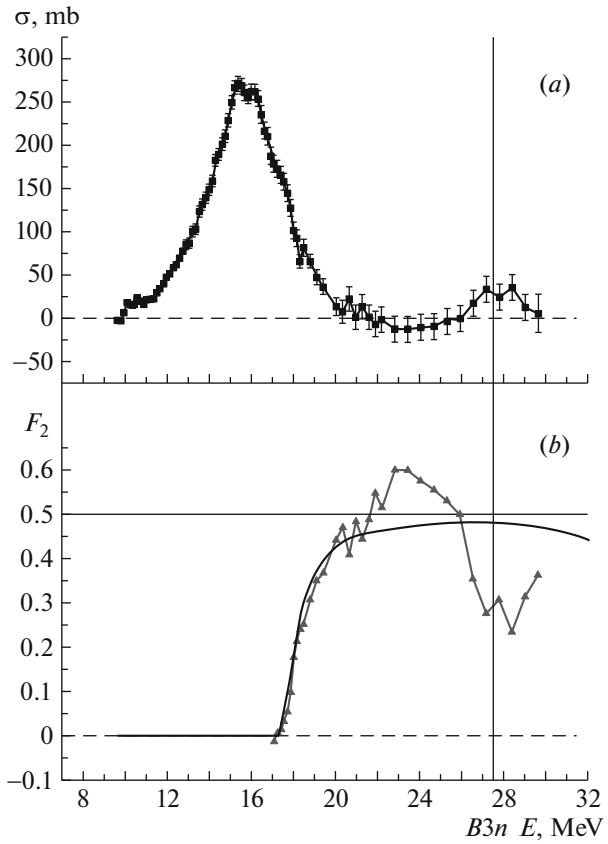

Fig. 6. Cross section obtained experimentally in Livermore [29] for the reaction $^{116}\mathrm{Sn}(\gamma, 1n)$ (closed boxes in Fig. 6*a*) and transition multiplicity function F_2^{exp} (closed triangles in Fig. 6*b*) versus energy. In either panel, the points are connected by a line in order to guide the eye. The curve in Fig 6*b* represents the function F_2^{theor} [32, 33].

model. It turned out that the evaluated cross sections differ substantially from their experimental counterparts, whose reliability is questionable, as was snown above.

For the ^{116}Sn nucleus discussed in the present study, the effects described above are illustrated in Fig. 6. Figure 6*b* shows that, precisely in the energy range between about 21 and 26 MeV, where the cross section of the reaction $^{116}\mathrm{Sn}(\gamma, 1n)$ has physically forbidden negative values, the function F_2^{exp} has values greater than 0.50, which is impossible by definition. This proves the unreliability of data obtained in this energy region for the cross section $\sigma(\gamma, 2n)$ and, hence, for the cross section $\sigma(\gamma, 1n)$.

The partial-reaction cross sections $\sigma^{\mathrm{eval}}(\gamma, in) = \sigma^{\mathrm{exp}}(\gamma, Xn)F_i^{\mathrm{theor}}(E_\gamma)$ evaluated with allowance for the reliability criteria by employing the experimental–theoretical method and the cross section evaluated according to Eq. (4) for the total photoneutron-production reaction are given in Fig. 7 along with

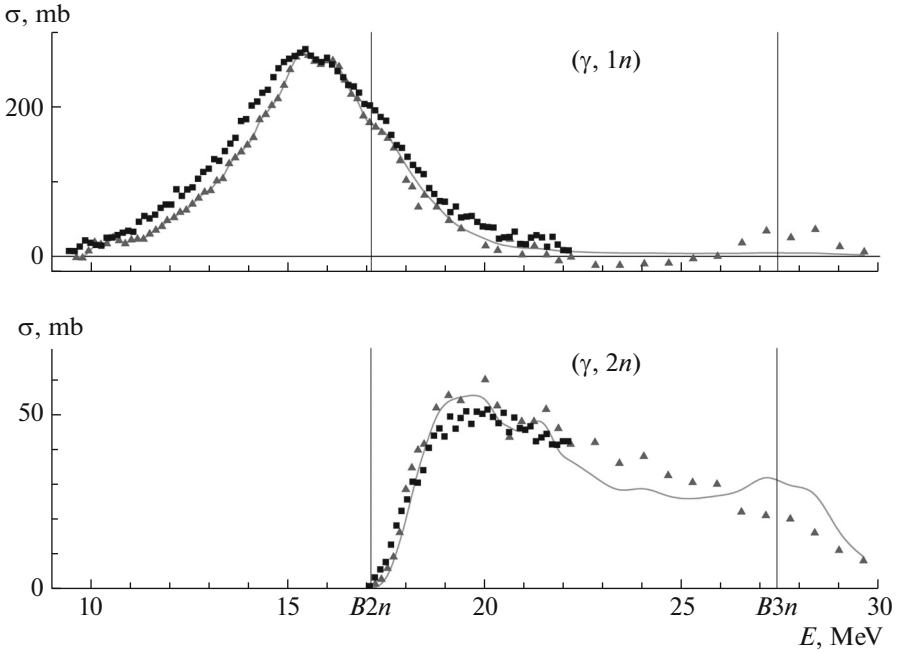

Fig. 7. Cross sections obtained experimentally for photoneutron reactions on ^{116}Sn nuclei in (closed triangles) Livermore [29] and (closed boxes) Saclay [30] along with (solid curves) their evaluated counterparts from [41].

respective experimental data obtained in Saclay [30] and Livermore [29].

One can see that, in accordance with the reliability criteria, the cross section evaluated for the $(\gamma, 1n)$ reaction in the energy range between about 21 and 26 MeV proves to be larger than the respective experimental cross section and has only positive values. At the same time, the cross section evaluated for the $(\gamma, 2n)$ reaction in this energy range proves to be substantially smaller (by about 20%) than the experimental cross section, and this leads to values of the ratio F_2 that do not exceed the physically reliable upper limit of 0.50.

In order to perform a more detailed comparison of the results of the calculations with the $(\gamma, 1n)$ and $(\gamma, 2n)$ cross sections measured experimentally, we have calculated the spectra of neutrons originating from the (γ, Sn), $(\gamma, 1n)$, $(\gamma, 2n)$, and $(\gamma, 3n)$ reactions at four values of the monoenergetic-photon energy: $E_\gamma = 20$, 23, 27, and 30 MeV. Figure 8 shows the total spectra of neutrons and the spectra of neutrons from the $(\gamma, 1n)$, $(\gamma, 2n)$, and $(\gamma, 3n)$ reactions. This figure gives the spectra of the first and second emitted neutrons from the $(\gamma, 2n)$ reaction and the spectra of the first, second, and third neutrons from the $(\gamma, 3n)$ reaction.

A decrease in the maximal and mean energies of each subsequent emitted neutron is a general regularity. As might have been expected, the energy of a major part of emitted neutrons is about 1 to 5 MeV. The Livermore detector records neutrons of such energy quite reliably. However, it should be kept in mind that the spectra in question contain neutrons of energy reaching its maximum value, which depends on the energy of the photon initiating the reaction being considered and on the threshold for this reaction. In the case of $E_\gamma = 20$ MeV, the maximum neutron energy is about 10.5 MeV, while, in the case of $E_\gamma = 30$ MeV, it reaches 20.5 MeV. The efficiency of the Livermore neutron detector was measured only up to about 5 MeV [12]. Since the neutron-detector efficiency becomes lower as the neutron energy increases, errors may arise in determining cross sections of $(\gamma, 1n)$ and $(\gamma, 2n)$ photoneutron reactions.

The total detector efficiency ε for recording neutrons at a given energy E_γ is used in Eqs. (8) and (9), which underlie the calculation of the reaction yields $Y(\gamma, 1n)$ and $Y(\gamma, 2n)$ on the basis of the numbers of counts, N_1 and N_2, in the outer and inner counter rings. This procedure ignores the fact that the neutron-detection efficiencies in the inner and outer rings behave differently as the energy of the detected neutron increases. While the efficiency of the inner ring becomes lower since fast neutrons do not have time to change before reaching it, the efficiency of the outer ring becomes higher owing to an increase in the number of neutrons that reached it. Therefore, it would be advisable to employ different efficiencies for the inner and outer counter rings. Moreover, the equations in question take into account only the possibility of the transition of part of the reaction

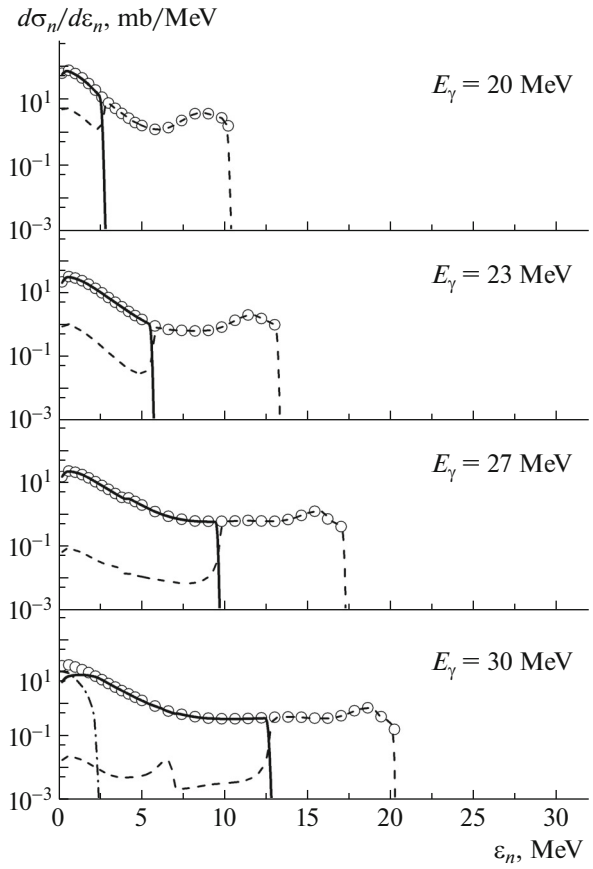

Fig. 8. Energy spectra of neutrons produced upon the decay of the states of the ^{116}Sn nucleus at the excitation energies of 20, 23, 27, and 30 MeV in the (dashed curve) $(\gamma, 1n)$, (solid curve) $(\gamma, 2n)$, and (dash-dotted curve) $(\gamma, 3n)$, and (dashed curve going through open circles) (γ, Sn) reactions.

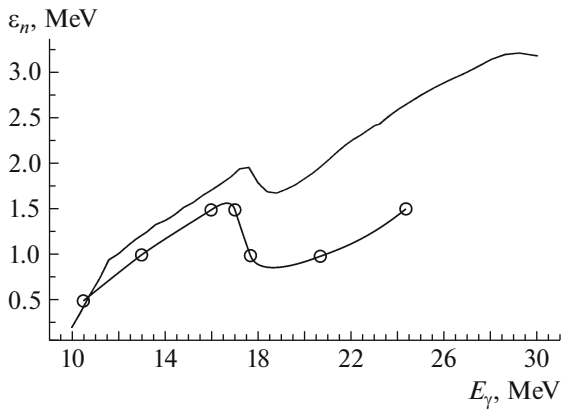

Fig. 9. Mean neutron energy ε determined in the experiment reported in [29] on the basis of the ring ratios (curve going through circles) along with the results of calculations based on the combined photonuclear-reaction model (solid curve) [32, 33].

yield $Y(\gamma, 2n)$ from the inner to the outer ring but disregards in inverse process—that is, the detection of part of the reaction yield $Y(\gamma, 1n)$ in the inner ring. It is precisely the disregard of this effect that leads to the drop of a segment of the $(\gamma, 1n)$ cross section to the the region of negative values (see Fig. 5 and 6).

The mean detected-neutron energy estimated with the aid of the "ring-ratio" method is obviously lower than the mean detected-neutron energy since the detector captures with a higher probability slow neutrons rather than fast neutrons. This circumstance is illustrated in Fig. 9, where the E_γ dependence of the mean detected-neutron energy [29] is contrasted against the analogous dependence of the mean emitted-neutron energy calculated on the basis of the combined photonuclear-reaction model. The dependences in question are similar in shape, but, as might have been expected, the theoretical curve goes substantially higher than the experimental curve. The discrepancy between them is especially great at high values of the energy E_γ. This indicates that the multiplicity sorting method for separating different partial reactions, which does in fact takes into account only the soft section of the photoneutron spectrum, may lead to substantial errors, especially at high values of the photon energy E_γ.

In addition, a determination of the E_γ dependence of the mean emitted-neutron energy on the basis of "ring-ratio" procedure is also open to criticism. In fact, this method makes it possible to determine the E_γ dependence of the mean ratio of ring populations rather than the analogous dependence of the mean emitted-neutron energy, but these two dependences are not identical since, in general, $\bar{f}(E_n) \neq f(\bar{E}_n)$ at a fixed value of E_γ.

Both the experimental ("ring-ratio" method) and the theoretical (calculation on the basis of the combined photonuclear-reaction model) results in Fig. 9 exhibit a decrease in the mean neutron energy for E_γ values between 17 and 18 MeV. This is due the opening of the $(\gamma, 2n)$ reaction channel.

In the region of energies above 18 MeV, the mean energy of neutrons increases. Although the two curves in question behave similarly in general, the calculation yields a substantially harder spectrum of emitted neutrons.

The neutron spectrum determined experimentally proves to be substantially softer than that which follows from theoretical calculations. In the region of energies around 23 MeV, where the excess of the transition multiplicity function F_2 above the physically admissible limit of 0.50 is maximal (see Fig. 6), the difference between the model and experimental results is about 1.25 MeV. This means that, in the experimental data, a substantially greater part of neutrons in relation to what we have in the model is assigned to the $(\gamma, 2n)$ reaction rather than to the

$(\gamma, 1n)$ reaction. It is precisely this difference in the mean energy of neutrons from the $(\gamma, 1n)$ and $(\gamma, 2n)$ reactions on the isotope ^{116}Sn that may be the reason for the difference in the above energy dependences of the cross sections of these reactions.

5. CONCLUSIONS

In comparing the results obtained by measuring cross sections in beams of bremsstrahlung photons and in beams of quasimonoenergetic photons, it should be kept in mind that, in experiments of either type, attempts at deducing reaction cross sections run into the same problem—immediately after the maximum of the cross section in (4) for the (γ, Sn) total photoneutron reaction, one extracts the result for the cross section as the difference of two commensurate values measured with a large statistical error [see Eq. (7)]. More reliable measurements of partial photoneutron reactions would require employing detectors that have a high neutron-detection efficiency in the neutron-energy range extending to 15 or even 20 MeV.

Prospects of further studies of partial photonuclear-reaction channels are expected to be dependent on future advancements along the following lines:

(i) It is necessary to develop methods that would permit directly identifying reaction channels. There is such a possibility in experiments where nuclei arising as reaction products are detected on the basis of the spectra of induced-activity gamma rays [42–44].

(ii) It is necessary to develop methods for directly measuring the spectra of neutrons and protons originating from photonuclear reactions.

(iii) Great hopes are pinned on the method for obtaining monoenergetic photons via the inverse Compton scattering of laser photons on accelerated electron beams. The basic advantage of this method is that, in contrast to what we have in spectrum of bremsstrahlung photons and the spectrum of quasimonoenergetic annihilation photons, the low-energy section of the spectra of inverse Compton scattering is strongly suppressed. This, along with a high energy resolution, would make it possible to improve substantially the accuracy in measuring cross sections at energies behind the maximum of the giant dipole resonance.

ACKNOWLEDGMENTS

We are grateful to D.V. Losev and N.N. Peskov for their help in obtaining and processing the data presented in this article.

This work was supported by Coordinating Research Project no. F41032 (research contract no. 20501) of the International Atomic Energy Agency (IAEA).

REFERENCES

1. A. B. Migdal, Zh. Eksp. Teor. Fiz. **15**, 81 (1945).
2. G. C. Baldwin and G. S. Klaiber, Phys. Rev. **71**, 3 (1947).
3. G. C. Baldwin and G. S. Klaiber, Phys. Rev. **73**, 1156 (1948).
4. M. Goldhaber and E. Teller, Phys. Rev. **74**, 1046 (1948).
5. M. Danos, Ann. Phys. (Leipzig) **10**, 265 (1952).
6. K. Okamoto, Prog. Theor. Phys. **15**, 75 (1956).
7. D. H. Wilkinson, Physica **22**, 1039 (1956); Physica **22**, 1043 (1956); Physica **22**, 1058 (1956).
8. J. P. Elliott and B. H. Flowers, Proc. R. Soc. London, Ser. A **242**, 57 (1957).
9. G. E. Brown and M. Bolsterli, Phys. Rev. Lett. **3**, 472 (1959).
10. V. G. Neudachin, V. G. Shevchenko, and N. P. Yudin, Sov. Phys. JETP **12**, 79 (1960).
11. J. Miller, C. Schuhl, and C. Tzara, Nucl. Phys. **32**, 236 (1962).
12. S. S. Fultz, R. L. Bramblett, J. T. Caldwell, and N. A. Kerr, Phys. Rev. **127**, 1273 (1962).
13. V. V. Varlamov, B. S. Ishkhanov, and I. M. Kapitonov, *Photonuclear Reactions. Current State of Experimental Research* (Univ. Kniga, Moscow, 2008) [in Russian].
14. B. S. Ishkhanov and I. M. Kapitonov, *Interaction of Electromagnetic Radiation with Atomic Nuclei* (Mosk. Gos. Univ., Moscow, 1979) [in Russian].
15. S. S. Dietrich and B. L. Berman, At. Data Nucl. Data Tables **38**, 199 (1988).
16. B. L. Berman, J. T. Caldwell, R. R. Harvey, M. A. Kelly, R. L. Bramblett, and S. C. Fultz, Phys. Rev. **162**, 1098 (1967).
17. R. A. Alvarez, B. L. Berman, D. D. Faul, F. H. Lewis, Jr., and P. Meyer, Phys. Rev. C **20**, 128 (1979).
18. E. Wolynec, A. R. V. Martinez, P. Gouffon, Y. Miyao, V. A. Serrão, and M. N. Martins, Phys. Rev. **29**, 1137 (1984).
19. E. Wolynec and M. N. Martins, Rev. Brasil. Fis. **17**, 56 (1987).
20. V. V. Varlamov, N. N. Peskov, D. S. Rudenko, and M. E. Stepanov, Vopr. At. Nauki Tekh., Ser.: Yad. Konst., Nos. 1–2, 48 (2003).
21. V. G. Solov'ev, *Theory of Complex Nuclei* (Nauka, Moscow, 1971; Pergamon, Oxford, 1976).
22. V. I. Isakov, Phys. At. Nucl. **79**, 811 (2016).
23. S. P. Kamerdzhiev and D. A. Voitenkov, Phys. At. Nucl. **79**, 904 (2016).
24. M. L. Gorelik, B. A. Tulupov, and M. G. Urin, Phys. At. Nucl. **79**, 924 (2016).
25. G. G. Adamian, N. V. Antonenko, A. N. Bezbakh, and L. A. Malov, Phys. At. Nucl. **79**, 951 (2016).
26. V. V. Balashov and V. M. Chernov, Sov. Phys. JETP **16**, 162 (1962).
27. A. P. Severyukhin, V. V. Voronov, and Nguyen Van Giai, Phys. Rev. C **77**, 024322 (2008).
28. Yu. I. Sorokin and B. A. Yur'ev, Izv. Akad. Nauk SSSR, Ser. Fiz. **39**, 114 (1975).

29. S. C. Fultz, B. L. Berman, J. T. Caldwell, R. L. Bramblett, and M. A. Kelly, Phys. Rev. **186**, 1255 (1969).
30. A. Leprêtre, H. Beil, R. Bergère, P. Carlos, A. de Miniac, A. Veyssière, and K. Kernbach, Nucl. Phys. A **219**, 39 (1974).
31. A. V. Varlamov, V. V. Varlamov, D. S. Rudenko, and M. E. Stepanov, INDC(NDS)-394, IAEA NDS (Vienna, Austria, 1999).
32. B. S. Ishkhanov and V. N. Orlin, Phys. Part. Nucl. **38**, 232 (2007).
33. B. S. Ishkhanov and V. N. Orlin, Phys. At. Nucl. **71**, 493 (2008).
34. M. B. Chadwick, P. Obloinský, P. E. Hodgson, and G. Reffo, Phys. Rev. C **44**, 814 (1991).
35. C. K. Cline and M. Blann, Nucl. Phys. A **172**, 225 (1971).
36. C. K. Cline, Nucl. Phys. A **210**, 590 (1973).
37. E. Gadioli, E. Gadioli Erba, and P. G. Sona, Nucl. Phys. A **217**, 589 (1973).
38. J. Dobes and E. Beták, Nucl. Phys. A **272**, 353 (1976).
39. V. V. Varlamov, B. S. Ishkhanov, V. N. Orlin, and V. A. Chetvertkova, Bull. Russ. Acad. Sci.: Phys. **74**, 833 (2010).
40. V. V. Varlamov, B. S. Ishkhanov, V. N. Orlin, and S. Yu. Troshchiev, Bull. Russ. Acad. Sci.: Phys. **74**, 842 (2010).
41. V. V. Varlamov, B. S. Ishkhanov, and V. N. Orlin, Phys. At. Nucl. **75**, 1339 (2012).
42. S. S. Belyshev, A. N. Ermakov, B. S. Ishkhanov, V. V. Khankin, A. S. Kurilik, A. A. Kuznetsov, V. I. Shvedunov, and K. A. Stopani, Nucl. Instrum. Methods Phys. Res. A **745**, 133 (2014).
43. S. S. Belyshev, A. A. Kuznetsov, K. A. Stopani, and V. V. Khankin, Phys. At. Nucl. **79**, 641 (2016).
44. H. Naik, G. Kim, K. Kim, M. Zaman, A. Goswami, M. W. Lee, S.-C. Yang, Y.-O. Lee, S.-G. Shin, and M.-H. Cho, Nucl. Phys. A **948**, 28 (2016).